Chapter 3

Optical Properties of Earth Surface Materials

3.1 Introduction

In this section, we look at the behavior of electromagnetic radiation in the optical or shortwave portion of the spectrum (from the visible to the SWIR). The optical portion of the spectrum refers to the portion of the spectrum that is directly dependent on solar energy and in which reflection processes are dominant over emission ones. The proportions of solar incident energy that are reflected, absorbed, and transmitted are a function of the unique characteristics of the surface and the wavelength at which it is being observed. A leaf will appear green if its reflectance at green wavelengths is greater than its reflectance in the blue or red portions of the visible spectrum. An object will appear blue if it reflects more energy in the blue region relative to the other wavelengths within the visible spectral region. The reflectance behavior of an object over the visible wavelengths results in what is called "color".

The relationship between the solar energy incident on a surface and the reflected energy that is remotely-sensed over various wavelengths reveals information about the state and composition of the surface. Specifically, remote sensing observations can provide quantitative information about the biogeochemical nature of the surface (canopy chemistry, soil mineralogy, water content) and the structural characteristics of the surface (e.g. canopy physiognomy, soil roughness). These may be referred to as the intrinsic properties of a surface.

The reflectance behavior of the surface as a function of wavelength throughout the optical portion of the spectrum is commonly referred to as a spectral reflectance signature or spectral fingerprint. In Figure 3.1, a series of laboratory- measured spectral reflectance signatures is shown representing various Earth surface materials. As can be seen, these commonly observed terrestrial surface targets, result in widely variable reflectance patterns over the different wavelengths. Snow exhibits very high reflectances in the visible region (blue, green, red). Color theory tells us that equal mixtures of blue, green,

and red yield a ‘white’ appearance. However, as we proceed to longer wavelengths, the reflectance of snow decreases dramatically, and snow begins to appear ‘black’ (near zero reflectance) over the SWIR wavelengths. Water, on the other hand, has low reflectances over the visible wavelengths with even lower or no reflectance in the near-infrared and greater wavelengths. These very low reflectance properties of water are a result of the high absorbing properties of water. The presence of sediments, pollutants, phytoplankton, and other materials in the water will alter the spectral signature of water, as shown in figure 3.1. Similarly, dust and pollutants will modify the spectral signature of snow. For the most part, these changes are predictable and allow for the use of remote sensing to assess the ‘age’ of snow and turbidity of water bodies.

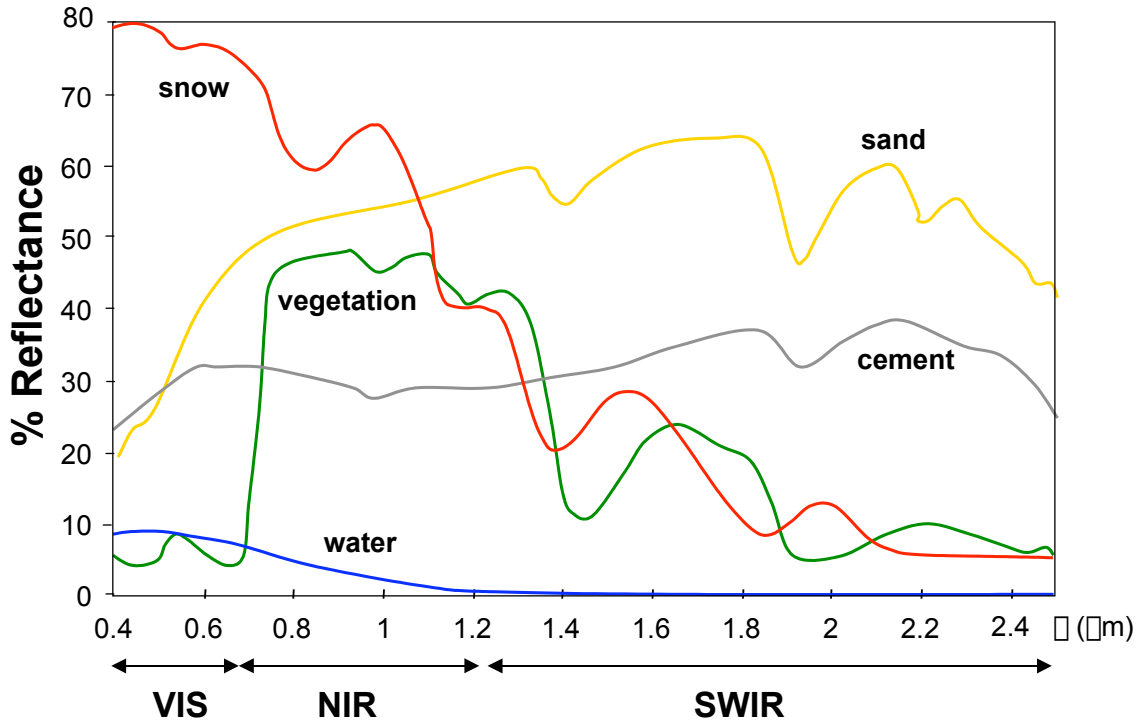

Figure 3.1. Spectral reflectance signatures for representative Earth surface materials.

The leaves of vegetation have very unique spectral reflectance signatures with low, but very chromatic, reflectances in the visible spectrum followed by a dramatic increase in reflectance in the near-infrared and lower reflectances again in the SWIR portion of the spectrum. Leaf spectral signatures are distinctly modified by leaf type and morphology, chlorophyll and water contents, plant vigor, stress, and senescence. At the

vegetation canopy scale, the amount and structural arrangement of the leaves will further influence the resulting reflectance. Soils, on the other hand, increase in reflectance gradually with increasing wavelengths in a manner dependent on their mineral (iron, salts), organic matter, and water content at the surface. A soil's spectral reflectance may be further modified by the morphologic and structural makeup of the surface, as well as by the presence of plant litter and its stage of decomposition.

In the following sections, we analyze in more detail the spectral behavior of typical land surface components, namely vegetation, soil, litter, and water. We discuss the optical properties of these materials and relate their spectral signatures to key biochemical and mineralogical components. The Earth's terrestrial surface will most likely contain many of the surface materials discussed above (soil, vegetation, water, litter) in varying proportions and arrangements and a remotely-sensed observation will often measure a mixed response of these multiple spectral signatures. Fortunately, there exist a wide variety of techniques in remote sensing aimed at extracting the basic, intrinsic properties of the surface from these mixed responses.

3.2 Vegetation Canopy Optical Properties

The optical characterization of vegetation canopies is one of the most important and challenging problems in remote sensing. The reflectance properties of a vegetation canopy are a result of many biochemical and biophysical canopy attributes as well as external factors that influence the signal detected at the sensor. A complete understanding of the optical behavior of a vegetation canopy includes the role of leaf biochemical, physiological, and morphologic properties. Leaf biochemical constituents include pigments, lignins, and water.

Electronic absorption processes at the molecular and atomic levels result in distinct leaf spectral features in the visible portion of the spectrum. Visible energy is absorbed by the various pigments present in a leaf, producing "color" changes with differences in pigment concentrations. Leaves also exhibit spectral features in the SWIR region caused by vibrational processes with liquid water. Plant physiologic stress associated with nutrient and water deficiencies result in different spectral signatures resulting from altered pigment and water related biochemical interactions. Leaf

morphology involves the external features of the leaves, such as size, shape, margins, and texture. Differences in leaf morphology have important effects in the resulting vegetation spectra which may include various plant classification criteria, e.g., needleleaf vs. broadleaf.

At the canopy level, one must also consider the structural properties of the canopy, such as physiognomy, fractional coverage, plant height, crown diameter, planting geometry, and association with other species. Finally, the physiological condition (vigor, phenology, stress) of the vegetation influences the final radiance signal at the sensor through its effect on chlorophyll levels and plant structure. Typically, many of the above vegetation properties will change simultaneously rendering it difficult to isolate one specific biophysical component. Aside from the vegetation canopy, there is also the underlying canopy background which may include such surface materials as soil, rock, litter, water, and snow. External to the canopy are various influences that alter the signal at the sensor including, sun illumination angle and sensor view angle, landscape topography (slope, aspect), and atmosphere effects.

In this section, we introduce the most basic and important aspects of vegetation optical properties. More rigorous treatments involving laboratory-based studies of leaf reflectance, optical-geometric models of plant canopies, and numerical radiative transfer canopy models can be found in Gates et al. (1965), Knipling (1970), Colwell (1974), Verhoef (1984).

3.2.1 Leaf Optics

The spectral characteristics of a leaf are mostly related to the activity of pigments in the visible region, leaf cellular structure in the near-infrared (NIR), and leaf water content in the shortwave-infrared (SWIR) (figs. 3.2). In the visible region (400- 700 nm), light absorption by leaf pigments dominates the reflectance spectrum and results in generally low reflectances (< 10%). The visible energy is strongly absorbed by the pigments chlorophyll (chlorophyll a and b), carotenoids (carotenes and xanthophylls), and anthocyanins, with the chlorophyll pigments accounting for 60-75% of the energy absorbed. There is strong chlorophyll absorption centered at about 650 nm (‘red’) and strong chlorophyll and carotenoid absorption centered at 450 nm (‘blue’). Between these

portions of the spectrum, there is a peak in reflectance in the 'green' region, at 550 nm, where the absorbing effect is smaller. This green peak is responsible for the green color of healthy vegetation and is indicative of healthy, actively photosynthetic leaves. The absorption behavior of chlorophyll generally masks the behavior of the other pigments, however, when chlorophyll production diminishes the other pigments are able to reveal themselves in various proportions, resulting in various leaf colors (Gates et al., 1965). In the fall (or end of the growing season), chlorophyll exerts a smaller influence as production decreases and the existing chlorophyll starts to break down. This allows the yellow/ orange pigment, carotene, and the red pigment, anthocyanin, to show, revealing an array of orange, red, and yellow leaf colors (e.g., grasslands become yellow).

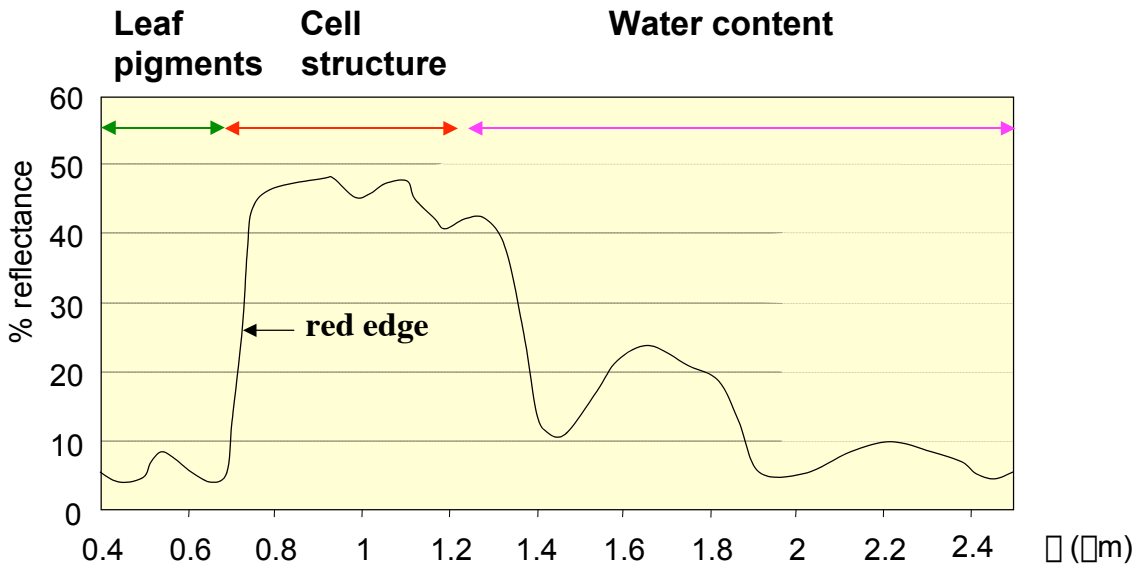

Figure 3.2. Leaf optical properties within the three optical domains.

Since most of the visible energy is absorbed by pigments to drive photosynthesis, the term 'photosynthetically-active radiation' (PAR) is used to describe the radiation in the visible part of the spectrum. Between the highly absorbing 'red' region and the highly reflective NIR is the sharp "red edge" region at around 740 - 780 nm. Plant nutrient and mineral stresses are known to cause shifts in the 'red edge'.

In the near-infrared (NIR) spectral domain (700-1300 nm), leaf structural properties play the dominant role in determining the leaf spectral signature. There is

strong reflectance between 700 and 1100 nm from the spongy mesophyll cells located in the interior of a leaf (fig. 3.3). Leaf pigments and cellulose are transparent to the NIR wavelengths resulting in very low leaf absorptance (<10%) and high leaf reflectance and transmittance values, approaching 50%. The NIR spectral domain has two main spectral portions; an NIR reflectance plateau between 700 and 1100 nm, where reflectance is very high, except in two minor water-related absorption bands (960 and 1100 nm); and a transition area between 1100 and 1300 nm, where reflectances decrease sharply from the NIR reflectance plateau to the low reflecting SWIR region (Fig. 3.2).

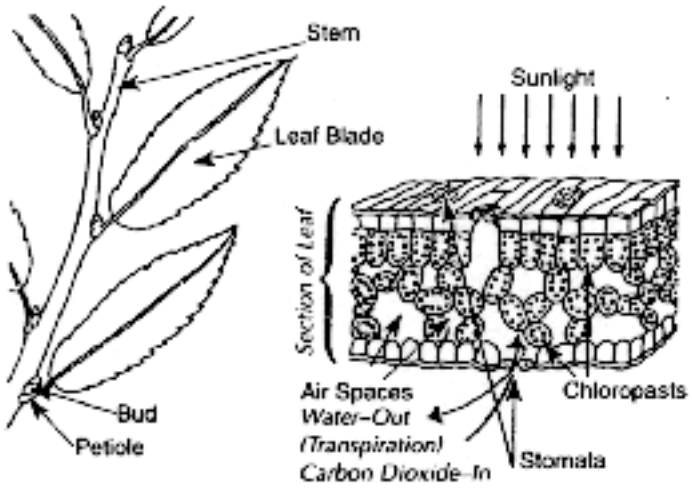

Figure 3.3 Basic components of a leaf and cellular structure.

The NIR reflectance plateau is dependent on the internal cellular structure of the leaf, particularly the thickness of the mesophyll layer. The spongy mesophyll layer, with its internal air cavities contains numerous air- water- interfaces with different refraction indices and the NIR wavelengths are multiply scattered until they eventually exit the leaf in upward (reflectance) or downward (transmittance) directions. Leaf reflectance in the NIR increases for more heterogeneous cell shapes and contents as well as with increasing number of cell layers, number of intercellular spaces, and cell size. Since leaf structure varies from species to species, the NIR is quite useful in discriminating among plants. As the magnitude of NIR reflectance is also generally greater in vegetation than from most inorganic materials, vegetation tends to be appear very bright and is easily recognized in NIR imagery.

The last optical domain is the shortwave infrared (1300 –2500 nm), which is dominated by leaf water absorption. Liquid water, which comprises 70-90% of the wet weight of leaves, strongly absorbs incident solar radiation in this range. Water strongly absorbs radiation at 1450 and 1950 nm, rendering these wavelengths so sensitive to water absorption that the water in the atmosphere prevents the energy at these wavelengths from reaching the Earth's surface. For this reason, reflectances in the SWIR region are generally measured outside these main absorption centers, over which leaf reflectances generally increase as leaf liquid water contents decrease (fig. 3.4). In the SWIR region, laboratory spectra show a large difference in leaf reflectance between dry and wet leaves (Knipling, 1970), especially in the wavelengths near 1400 nm and 1900 nm. In experiments with fig tree leaves, the reflectance of the dry leaf was up to four times the value of the wet leaf near the 1.9 μm absorption region. In other studies involving conifer leaves, as the leaves began to dry up, a slight increase in reflectance was observed in the SWIR, whereas slight decreases were observed in the NIR, and no variations were noticeable in the visible bands (Westman and Price, 1988). Remotely-sensed observations in the SWIR are thus of great in studies of leaf water content.

Figure 3.4. Leaf spectral signatures as a function of moisture content.

The overall spectral signature of a leaf or plant is further affected by leaf age, nutrient stress, diseases, vigor, and leaf morphology. Vegetation stress will cause

significant changes in plant spectral signatures. The senescent or stressed leaf immediately reduces chlorophyll activity resulting in less absorptance in the red band with slight decreases in blue absorption (since carotenes persist and continue to absorb in the blue). The consequent increase in red reflectance and slight increase in blue reflectance, alters the proportion of reflectance in the primary colors (blue, green, red) resulting in a change in leaf color towards a yellowish color. In the NIR, a reduction in leaf reflectance may take place with stress, due to the deterioration of the cellular structure of the leaf. The spectral curve, therefore, becomes flatter and less chromatic (Knipling, 1970). Such information has been shown to be valuable in detecting damage produced by forest plagues (disease) or fires.

In other studies, a clear relation between the ratio, NIR/ SWIR, and the humidity content in the leaves has been shown, providing a mechanism for the determination of areas affected by water stress (Cohen, 1991; Hunt and Rock, 1989). In addition, a displacement in the red edge towards shorter wavelengths has been observed and associated with leaf stress. This phenomenon was observed with plants affected by heavy metal contamination.

3.2.2 Canopy Optical- Geometric Properties

In scaling up from the individual leaf to the vegetation canopy, one needs to consider the grouping, arrangement, and amount of leaves within a canopy. The structural arrangement of the leaves alters the spectral signature of the component leaves and influences the overall radiant energy transfer through the canopy. Canopy optical-geometric properties include, canopy structure and architecture, physiognomy (grass, shrub, tree), plant height, crown diameter, leaf angle distribution (LAD), leaf area index (LAI), ground cover fraction, "clumping" and spatial heterogeneity, species composition, and the underlying soil and litter background. Solar radiation may be absorbed, reflected, or transmitted through the individual plant leaves and onto the soil surface, where it is either reflected or absorbed. Since NIR transmittance through a leaf approaches 50%, the amount of lower leaves will have an influence on the NIR reflectance signal at the top of the canopy. Similarly, the brightness of the soil will affect the remotely-sensed signal, even in fully vegetated (100%) surfaces.

Identifying vegetation types in remote-sensing images relies on several of these optical-geometric plant characteristics. For instance broadleaf trees with large, planar leaves, tend to be more reflective than the needle-line evergreen trees, particularly in the NIR. This aides in the spectral discrimination of forest cover types in spaceborne imagery. Crop identification in agricultural fields can, at times, be differentiated based on plant architecture. Soybeans have spread out leaf clumps; corn has tall stalks with long, narrow leaves and thin, tassle-topped stems; and wheat has long thin central stems with a few small, bent leaves on short branches, with a head containing kernels. Other optical-geometric related differences include plant height and the amount of shadow it casts; row spacing, orientation, and other planting geometries; and stage of growth, phenology, and extent of crop maturity. In shrublands, the size and shape of the more densely vegetated clumps amidst a bare soil or grass backgrounds create unique optical-geometric reflectance patterns.

Despite the great complexity in fully understanding vegetation canopy optics, as outlined above, there are many common traits present in most vegetation canopy spectra, such as the high contrast observed in the spectral reflectance curves between the visible region, especially in the red band (around 650 nm), and the near-infrared region (700 to 1300 nm). In general, one can say that the greater the contrast between these two regions, the greater the amount and vigor of the vegetation. In fact, the theoretical spectral behavior of vegetation in the 'red' and NIR forms the basis for the design and development spectral vegetation indices, which are constructed from combinations of these two bands (ratios, linear sums, etc.). They are designed to isolate and enhance the vegetation signal in remotely-sensed imagery, thereby facilitating the discrimination and extraction of useful vegetation information (Tucker, 1979).

3.3 Soil Optical Properties

Much is known about soil optical properties through extensive laboratory and *in-situ* field measurements. In contrast to vegetation, there is very little transmission of electromagnetic energy through the opaque soil medium. Liang (1997) found the sensible depth to be only 4-5 times the particle size effective radius. The spectral composition of soil-reflected energy is mostly dependent on the biogeochemical (mineral

and organic) constituents, geometrical-optical scattering (particle size, aspect, roughness), and moisture conditions of the immediate soil surface (Ben-Dor et al., 1999; Irons et al., 1989; Baumgardner et al., 1985).

3.3.1 Biogeochemical Properties

Soil spectral reflectance signatures result from the presence or absence, as well as the position and shape of specific absorption features of its constituents (fig. 3.z). Absorptions are brought about by various chemical/physical phenomena such as intermolecular vibrations and electronic processes in atoms. The visible and near-infrared (VIS-NIR) regions (0.4 μm - 1.3 μm) are characterized by broad spectral absorption features, such as the yellowish, ferrous iron absorption feature near 1 μm, and weaker absorptions at 0.7 μm and 0.87 μm attributed to red, ferric iron. Strong Fe-O charge transfers in the blue and ultraviolet result in fairly steep decreases in reflectance with shorter wavelengths. As a result, most soils exhibit increasing reflectance with wavelength over the visible to NIR portion of the spectrum, since iron is fairly ubiquitous (Mulders, 1987). Soils have distinct spectral features in the shortwave-infrared (SWIR) region (1.3 μm - 2.5 μm) caused by vibrational processes, which include two broad water absorption bands at 1.4 μm and 1.9 μm. Minerals with OH, CO_3 (calcite), and SO_4 (gypsum) exhibit vibrational features in the 1.8 μm to 2.5 μm region, while layer silicates with OH absorb near 1.4 μm and 2.2 μm (Baumgardner et al. 1985; Mulders, 1987).

Soils are mixtures of a number of inorganic and organic constituents so it is not straightforward to evaluate the composition of soils from their spectral signatures. Many soil spectral signatures match closely, making it difficult to distinguish them. As a result, only a limited number of soil spectral curve forms have been found discriminable with remote sensing. Condit (1970) analyzed 160 soil spectral reflectance curves, from 0.32 to 1.0 μm, and found only three principal spectral curve shapes. Stoner and Baumgardner (1981) analyzed a greater number and geographic range of soils (485 soils), from 0.50 to 2.45 μm, and documented five unique soil spectral curve shapes primarily related to their relative contents in organic matter and iron and modulated by their textures (Fig. 3.5). These, along with numerous laboratory and field studies have shown that soil spectral

signatures are largely controlled by the iron oxides, organic molecules, and water that coat soil particle surfaces. The curve forms represent; (1) minimally altered soils with both low organic matter and low iron contents; (2) organic dominated soils with high organic matter contents and low iron contents; (3) iron affected soils with low organic matter contents and medium iron contents; (4) organic affected soils with high organic matter contents, not fully decomposed, and low iron contents; and (5) iron dominated soils with high iron contents and lower organic matter amounts.

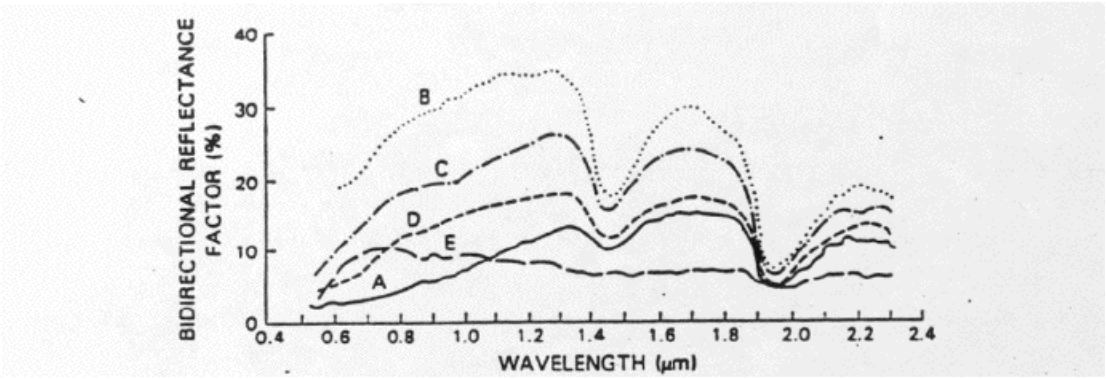

Figure 3.5 Five basic soil spectral curve shapes (Stoner and Baumgardner, 1981)

3.3.2 Soil Moisture

Soil moisture has a strong influence on the amount and composition of reflected energy from a soil surface and thus, information about soil moisture condition can be derived from measurements in the optical portion of the electromagnetic spectrum (Fig. 3.6). In the shortwave region, the major effect of adsorbed water on soil reflectance is a pronounced decrease in reflected energy making soils darker when moistened, particularly in the water absorption bands centered at 1.45 μm and 1.9 μm. The decrease

in reflectance is proportional to the thickness of the water film around the soil particles and can be related to the gravimetric water content as well as energy status of the adsorbed water. The SWIR region is considered the most sensitive to surface moisture content and remotely-sensed observations in this region offer potential soil water indicators. Water absorption in the SWIR has been related to soil water content for discrete soil textural classes (Musick and Pelletier, 1988).

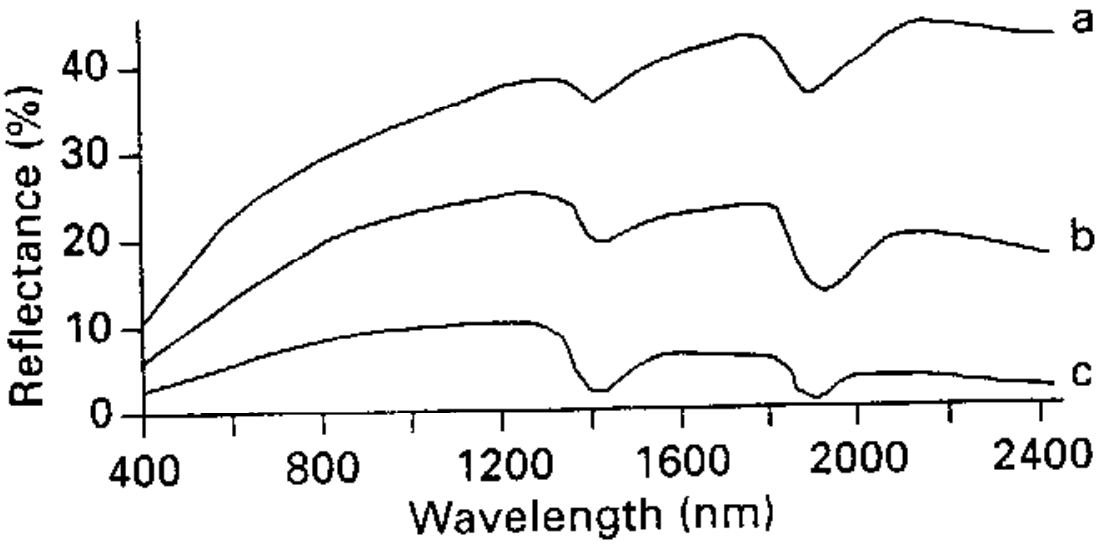

Figure 3.6. Soil reflectance curves as a function of water content, (a) 5%, (b) 20%, and (c) 40% water content. (Stoner and Baumgardner, 1981).

3.3.3 Optical - Geometric Considerations

Particle size distribution and surface-height variation (roughness) are the most important factors influencing the reflectance of bare soils. They cause a decrease in reflectance with increasing size of ‘roughness elements’ as coarse aggregates contain a lot of interaggregate spaces and 'light traps'. Smooth, crusted, compacted, and structureless soils generally reflect more energy and are brighter. Clayey soils, despite having a finer particle size distribution, tend to be darker than sandy soils since clays aggregate and behave as larger, "rougher" surfaces.

3.4 Litter and non-photosynthetic vegetation (NPV)

The presence of leaf litter and other non-photosynthetic vegetation (NPV) material on the soil surface influences the resulting soil spectral signatures as well as overall vegetation canopy reflectance properties. Many studies have investigated the chemical and optical properties of soil organic matter dynamics as a function of plant source and aging (Aber et al., 1990). Stoner and Baumgardner (1981) showed three unique spectral signatures representative of various stages of litter decomposition in soils (fig. 3xx). A 'fibric' curve had the most tissue morphology intact and thus high reflectance properties. 'Hemic' curves resulted from intermediate levels of decomposition, while 'sapric' curves represented mostly decomposed litter and were very low reflecting. Ben-Dor et al. (1997) found that the slopes in the VIS-NIR spectral region and specific absorption features in the NIR-SWIR region were useful in assessing the optical properties of soil organic matter at several stages of biological decomposition. McLellan et al. (1991) used a near-infrared analysis (NIRA) methodology to predict the amounts of nitrogen, lignin, and cellulose during the decomposition process of leaf materials to soil organic matter.

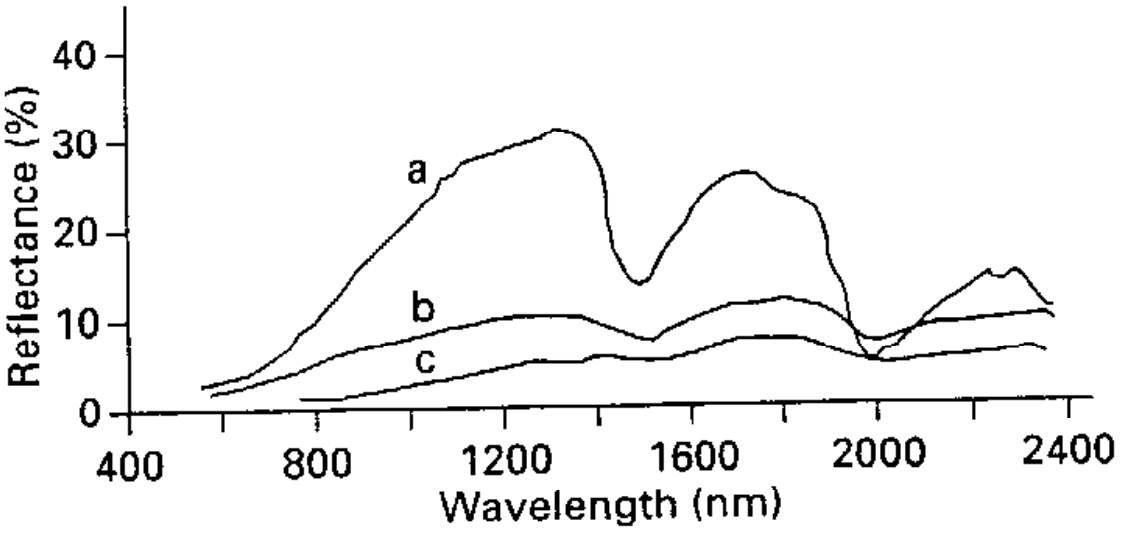

Figure 3.7. Soil organic matter reflectance curves, (a) minimally decomposed plant material; (b) partially decomposed; and (c) completely decomposed. (Stoner and Baumgardner, 1981)

Non-photosynthetic vegetation also includes the woody material found in standing vegetation, such as in savannas, shrublands, and forests. The spectral signatures of soils and litter/ NPV are often difficult to discriminate (Nagler et al., 2000), however, Asner and Lobell (2000) developed a spectral technique to distinguishing NPV from both soils and vegetation in the the SWIR. They used three narrow bands centered at 2080 nm, 2210 nm, and 2270 nm, with the first band chosen as a reference point, the second to distinguish soil from plant material, and the third to separate litter from the green canopy signal. We will discuss this more in a later chapter.

Our final spectral reflectance signature for a vegetated canopy consists of leaf biochemical and canopy structural (optical-geometric) components. Mixing into this spectral signature are the biogeochemical components of senesced vegetation, litter, soil organics and mineralogy, woody stems, bark, and other non-photosynthetic landscape materials. The biogeochemically "mixed" signal can be analyzed through the use mixture modeling, principal components analysis, spectral indices, and radiative transfer models. These will be studied in later chapters.

3.5 Water in the Optical Spectrum

Water bodies and aquatic surfaces absorb or transmit most of the radiation they receive. The greater the wavelength, the greater the absorptance. The spectral reflectance signature of water is opposite to that of soil with the highest reflectance in the blue band, and a gradual decrease in reflectance towards the near- and shortwave-infrared, where it becomes practically zero. For this reason, the borders between terrestrial surfaces and water bodies are well delineated in the SWIR region.

The variance in water spectral patterns is readily detected in the shorter wavelengths (blue and green). This is related to the depth of water, content of materials in suspension (chlorophyll, clays, and nutrients), and roughness of the surface. Suspended sediments in water result in reflectance increases in the visible wavelengths, this being a function of the particle size of the suspended elements (Bhargava and Mariam, 1990). The depth of the water influences the reflectance contribution from the materials at the bottom of the water. Reflectances are greater in shallow waters, since the reflectance of the bottom gets mixed with the water signal. The greater the water depth,

the higher the overall absorptance. In a study involving the use of Landsat imagery, it was found that the maximum water depth detectable was 6.4 meters in the blue band, 3 meters in the green, and 2 meters in the red (Ji et al., 1992).

Several studies have demonstrated the use of satellite imagery to assess chlorophyll content in water bodies (Lopez and Caselles, 1989). The greater the concentration of chlorophyll, the lower the reflectance in the blue band with simultaneous increases in the green band. This pattern has been used to locate the buildup of algae and seaweed and to the study processes of eutrophication in dams. In an optical- geometric sense, the roughness of the surface results in greater reflectances. Calm waters, on the other hand, reflect solar incident energy in a single direction (specular reflection) whereas rough surface diffusely scatter the solar radiation.

Snow, on the other hand, has a very different spectral behavior to that of water (fig. 3.8). Snow has a very high reflectance in the visible bands, decreasing in the near-infrared, and even more so in the SWIR wavelengths. The most important determinant of snow reflectance are, snow grain size, snow depth, density of the snow layer, and the amount of impurities it contains (Dozier, 1989). The reflectance is highest for fresh snow than for frozen snow, and the lowest values correspond to dirty snow (fig. 3.8). This decrease can reach up to 80 % in the visible bands (Hall and Martinec, 1985).

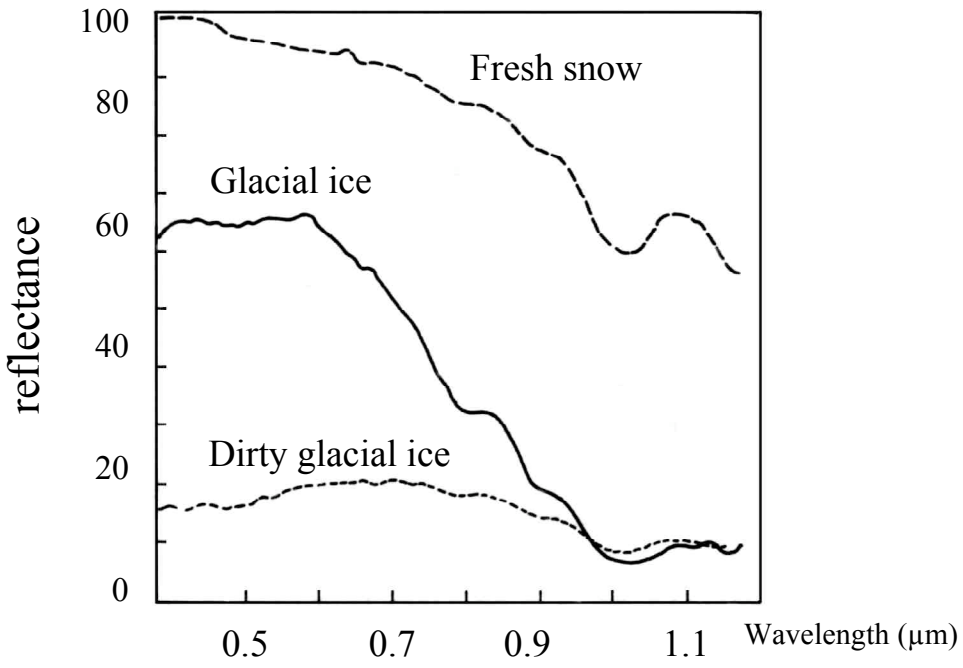

Figure 3.8. Reflectance curves for different types of snow and ice (Hall and Martinec, 1985).

3.6. External Factors

In extending the surface component spectral signatures to the satellite sensor, one must consider some additional factors that influence the energy received at a sensor and which render the interpretation of remotely-sensed data more complicated. The measured signal will likely consist of mixtures of two or more components (e.g., soil, litter, green vegetation, NPV) in varying proportions depending on the land cover type and stage of the growing season. There are also important external influences that need to be accounted for such as the atmosphere between the sun and the surface and the surface and the sensor, the sun-surface-sensor geometry of the observation, topography considerations, and sensor characteristics such as instrument calibration and filter response functions. Thus, the observed response from the surface is influenced not only by its own inherent, reflectance properties, but also by a series of external factors that modify the spectral signature of a surface. Some of these factors include (fig. 3.9):

- Solar angle of illumination (i), which varies with the day of the year, time of the satellite overpass, and latitude of the surface.
- Modifications that the terrain introduces to the observation geometry, namely aspect (ii) and slope (iii).
- Influence of the intervening atmosphere and clouds (iv), including selective scattering and absorption over different wavelengths.
- Environmental variations in the surface cover (v) as related to spatial heterogeneity and temporal phenology.
- Soil- vegetation interactions (vi), which are particularly dominant in open canopies characteristic of subhumid and semiarid lands.

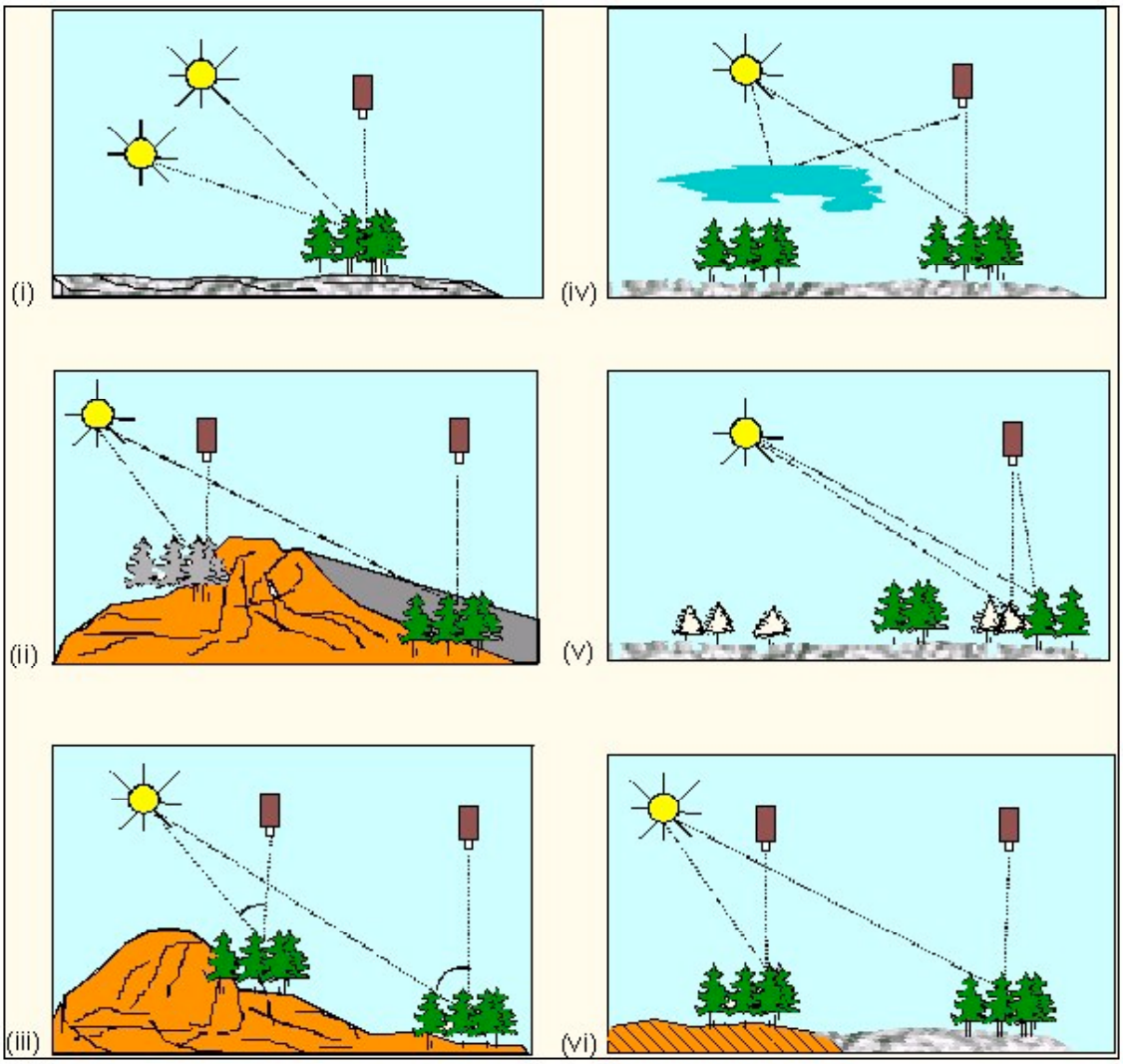

Figure 3.9. Factors influencing the spectral signatures of vegetation canopies, (i) sun angle (i); topographic aspect (ii) and slope (iii); atmosphere (iv); phenology (v); and soil-vegetation interactions (vi).

All of these factors show the complexity involved in the discrimination and characterization of land surface conditions using remote sensing. Thus, a land surface cover type does not necessarily exhibit a single, unique spectral response, that coincides with their leaf-based spectral reflectance signature. Each cover type will have considerable spectral variability, due to the factors mentioned above, and which adds difficulty to their discrimination.

In spite of this, pure component spectral reflectance curves have much utility in image interpretation and they provide a mechanism to relate the values acquired by the

sensor to the surface properties. Furthermore, pure component spectral signatures act as *endmembers*, allowing us to unmix the sensor signal and enable us to design optimal bands and band combinations for land surface features discrimination. The extraction of the surface-dependent spectral signatures and surface properties from the modified signal received at the sensor is a primary goal of remote sensing data processing, which may include correction for many of these influences.

3.6.1 Observation geometry

The amount and composition of energy reaching a sensor is dependent on the geometric conditions of an observation, in particular, the angle of solar incidence, the angle of observation, and their azimuthal orientation (fig. 3.10). Variations in observation geometry result in different radiance values at the sensor as well as computed surface reflectance values for a given surface condition. Seasonal and latitudinal variations in reflectance will be partly a function of the changing illumination conditions (sun angle and azimuth) with latitude that further vary seasonally over the year for a given location.

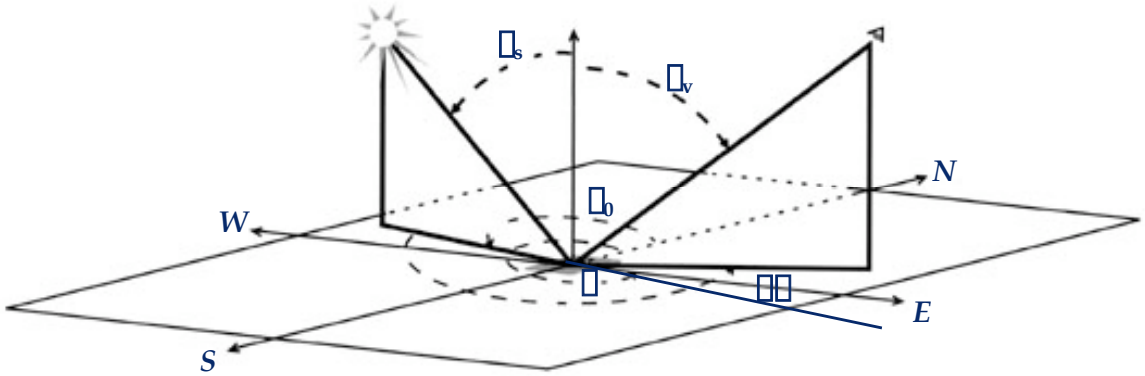

Figure 3.10. Definition of Solar Zenith (θ_s), View Zenith (θ_v), and Relative Azimuth Angle (ϕ).

The geometry of the observation is closely linked to the roughness of the surface and the way the surface is illuminated and shadowed by the sun. Most terrestrial surfaces scatter incident radiation anisotropically, a consequence of its three dimensional structure

and the resulting scattering behavior. Two types of surface scattering conditions may be depicted (fig. 3.11); those that reflect incident energy at the same angle as the incident angle (specular reflection), and those that scatter energy diffusely in all the directions. In the first case, the sensor receives a reflected energy response from the ground if it is located in the direction of the reflection angle. If the surface is diffuse, the radiance is reflected in all directions. A perfectly diffuse surface reflects energy equally in all directions (isotropic), however, most surfaces have anisotropic reflectance characteristics in which the reflected energy varies with the observation angle. A surface in which the reflected radiance, L, is constant for any angle of reflection (independent of viewing angle) is known as a Lambertian surface.

Most land surfaces exhibit anisotropic reflectance behavior with some diffuse and specular types of scattering which are dependent on their surface characteristics and on the wavelength involved. At shorter wavelengths, the roughness of the surface will be more pronounced and incident energy will be more diffusely scattered compared with incident energy scattering at greater wavelengths, where the surface will appear 'smoother' and more prone to specular behavior. For example, in the visible part of the spectrum, only calm water results in specular reflection, while most other surfaces (rough waters, vegetated canopies) will reflect diffusely. In the microwave part of the spectrum (greater wavelengths), many other surface covers can behave in a specular fashion, since the roughness of the surface will be relatively smaller.

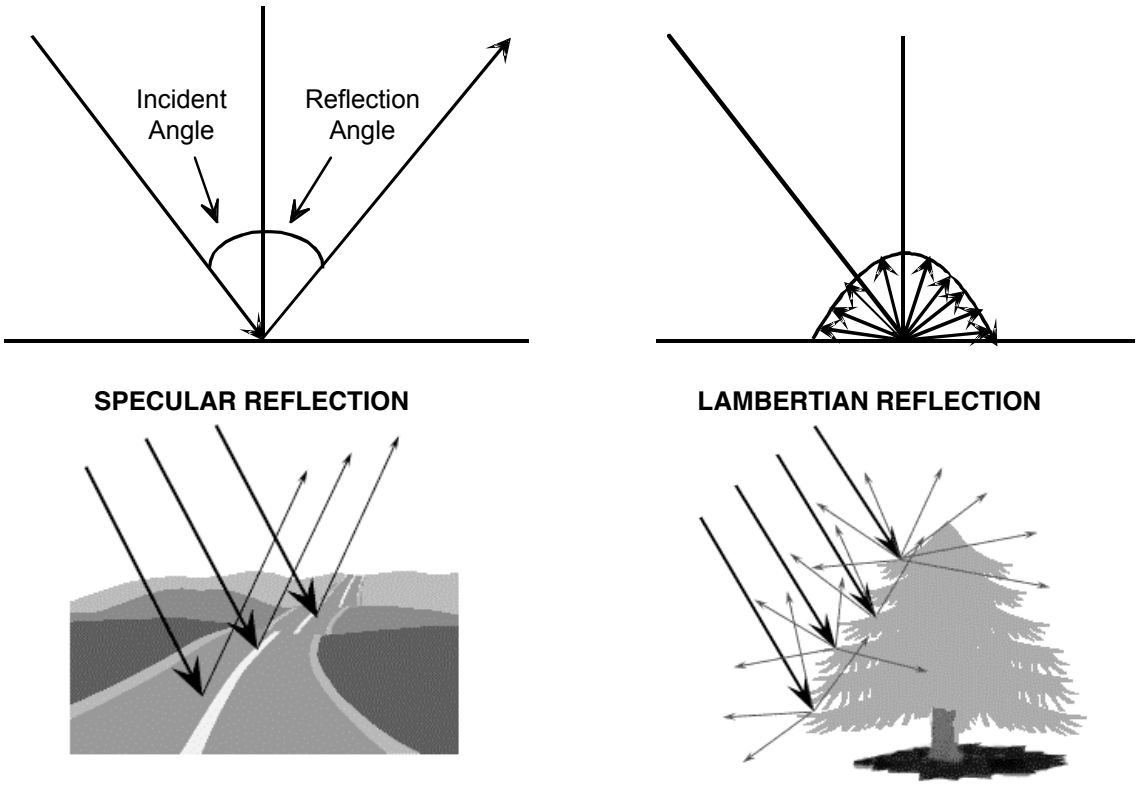

Figure 3.11. Different types of reflection- scattering processes with the Earth's surface.

A fundamental and intrinsic property governing the reflectance behavior of a surface is described by the Bidirectional Reflectance Distribution Function (BRDF), which specifies the behavior of surface reflectance and scattering as a function of view and illumination angles for a given wavelength. The equation describing this function is:

$$BRDF = L(\theta_s, \phi_s, \theta_v, \phi_v, \lambda) \; / \; E(\lambda), \qquad [3.1]$$

with units of sr^{-1}. θ_s and ϕ_s refer to the solar zenith angle and solar azimuth, respectively, while θ_v and ϕ_v are the sensor view zenith and view azimuth angles, respectively. Often, however it is defined simply as the bidirectional reflectance factor (BRF = πBRDF) at a multitude of view zenith and azimuthal angles for a given sun position (Walthall et al., 1985). The BRDF is an intrinsic physical property of the surface that may be used to derive geometric descriptors of a surface, such as size, shape, and orientation of surface

"roughness" elements. Examples of BRF patterns for ocean and tundra surfaces are included in figures 3. 12 through 3.15.

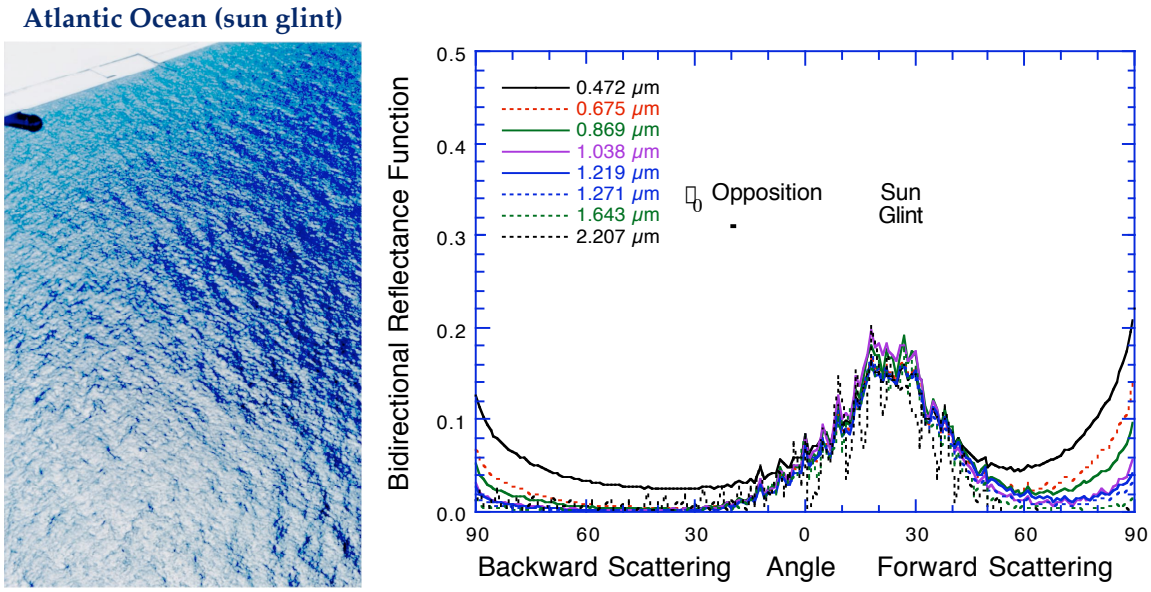

Figure 3.12. Bidirectional reflectance factor profile of an ocean surface for various wavelengths. Note the presence of a strong specular component (sun glint) as well as diffuse scattering.

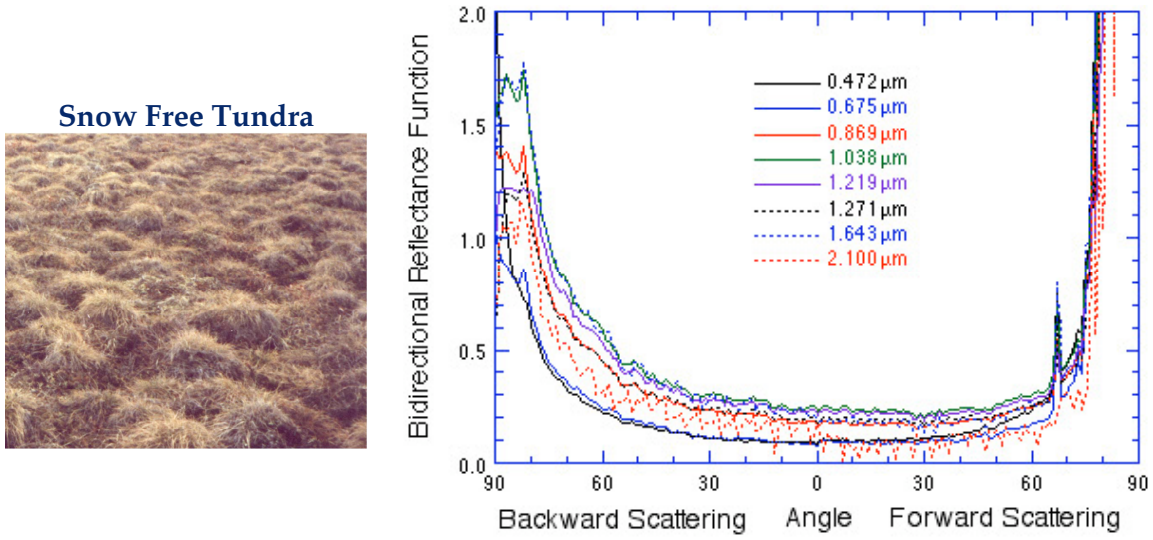

Figure 3.13. Bidirectional reflectance factor spectra of a snow free tundra surface for various wavelengths.

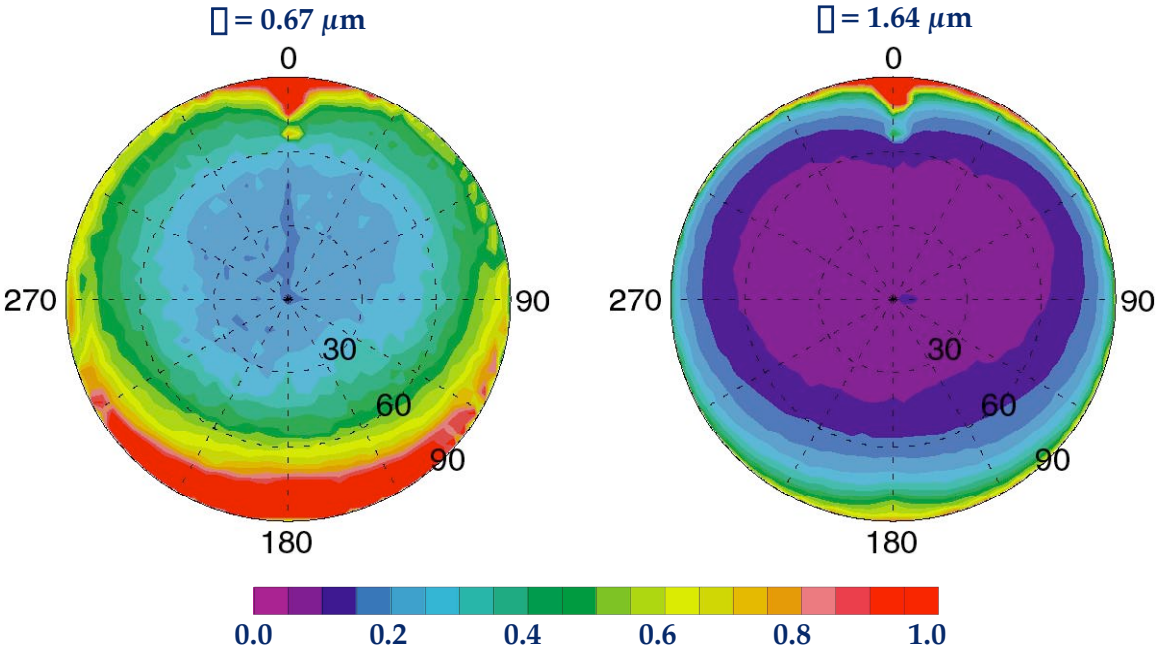

Figure 3.14. BRDF-fingerprint of snow free tundra surface depicting the distribution of reflectance values as a function of view zenith and azimuth angles for two wavelengths and a sun zenith angle of 81°.

In figure 3.15, we can observe a barren soil field from a constant view and sun zenith angles but from two azimuthal angles, 180º apart. The soil surface is significantly

brighter (more reflective) when viewed with the sun behind the sensor while the soil surface becomes much darker when viewed with the sun directly in front of the sensor. These two azimuthal directions are commonly termed, the backscatter and forward scatter directions, respectively. When the view azimuths are along the same plane as the sun, we term this the "principal plane", i.e., the relative difference in azimuth between sun and sensor, $\Delta\phi$ is 0 or 180º (see figure 3.10).

Figure 3.15. Viewing a bare soil field at a constant view and sun zenith angles, but opposite azimuthal angles, i.e, 180º apart.

Remote sensing data taken under different sun and viewing geometries are not necessarily comparable without correction for these angular effects. Knowledge of the BRDF of a surface allows for the correction of angular reflectance variations by normalizing responses to a given viewing geometry, such as nadir. When integrated across a hemisphere, the BRDF provides "albedo", the ratio of shortwave (0.4 μm to 4 μm) radiant energy scattered in all directions to the downwelling irradiance incident on the surface. Albedo is a fundamental variable in energy balance studies, climate modeling (Middleton et al., 1987), and soil degradation studies.

3.6.2 Role of the atmosphere in the optical domain

Up to now we have considered the interaction of electromagnetic radiation with the land surface as if this process were occurring in a vacuum. However, between the sun and terrestrial surface as well as between the surface and the satellite sensor, there is an intervening atmosphere through which the solar irradiance and the surface reflected radiance must pass through. The atmosphere influences and interferes with the radiant flux in different ways, but primarily through scattering and absorption processes. These processes alter the resulting spectral irradiance and spectral reflectance signatures.

The atmosphere, consisting of various gases and aerosols, behaves as a selective filter and spectrally modifies both the irradiance and reflected radiance signatures. Absorption processes in the optical region are related to 7 main gases present in the atmosphere, namely carbon dioxide (CO_2), oxygen (O_2), ozone (O_3), nitrous oxide (N_2O), carbon monoxide (CO), methane (CH_4), and water vapor (H_20) (fig. 3.16). These gases affect approximately half of the 0.4 to 2.5 μm, optical region. The strong water absorption bands at 1.45 and 1.95 μm completely attenuate solar energy and render these wavelengths useless for the study of the land surface from space. Ultraviolet sensing of the land surface also cannot occur due to strong O_3 absorption. In addition to these gases there are also aerosols, which may consist of smoke, salt spray, water droplets, etc. An aerosol is a dispersion of solid particles (smoke, smog, and dust) and/or liquid particles (haze and fog) suspended in air.

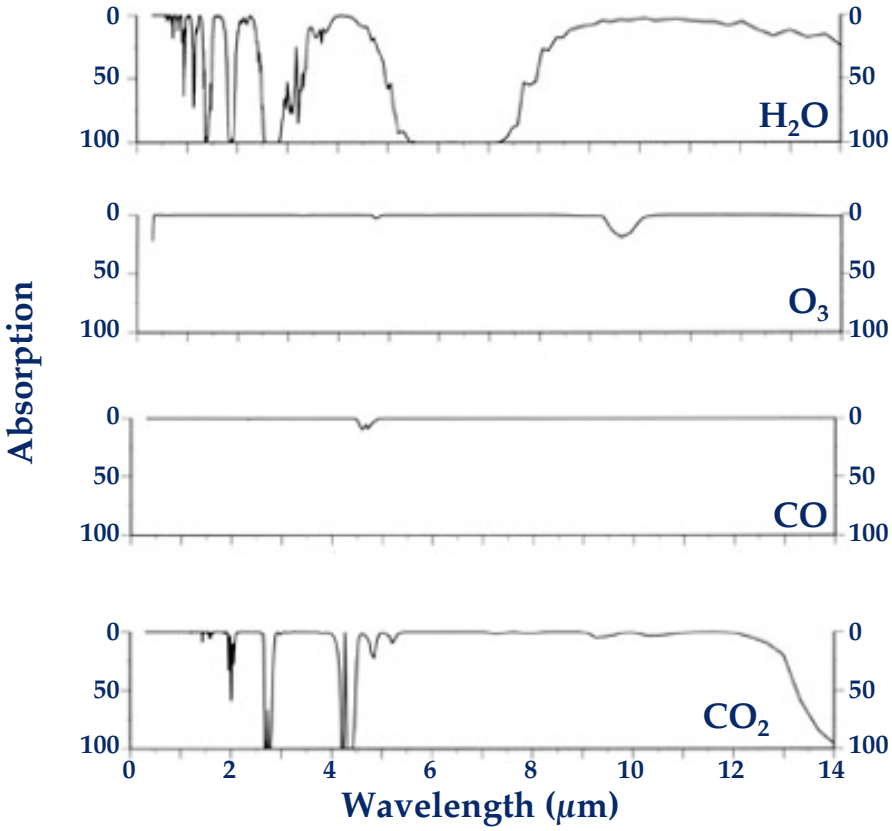

Figure 3.16a. Atmosphere absorption by atmosphere gases.

Among these components, carbon dioxide, ozone, and water vapor are the main gases influencing the interaction of electromagnetic energy with the atmosphere. The main gases and absorption regions include:

- Atomic oxygen (O_2), which filters the ultraviolet radiation below 0.1 □m, as well as small portions in the thermal infrared.
- Ozone (O_3), which absorbs ultraviolet energy below 0.3 μm as well as in a portion of the microwave region at around 27 □m.
- Water vapor (H_2O) with strong absorptions at 1.45 µm, 1.95 µm, and 6 □m with minor absorptions in the near-infrared.
- Carbon dioxide (CO_2), which absorbs in the thermal infrared (15 μm) and with important absorption effects in the shortwave infrared, between 2.5 and 4.5 μm.

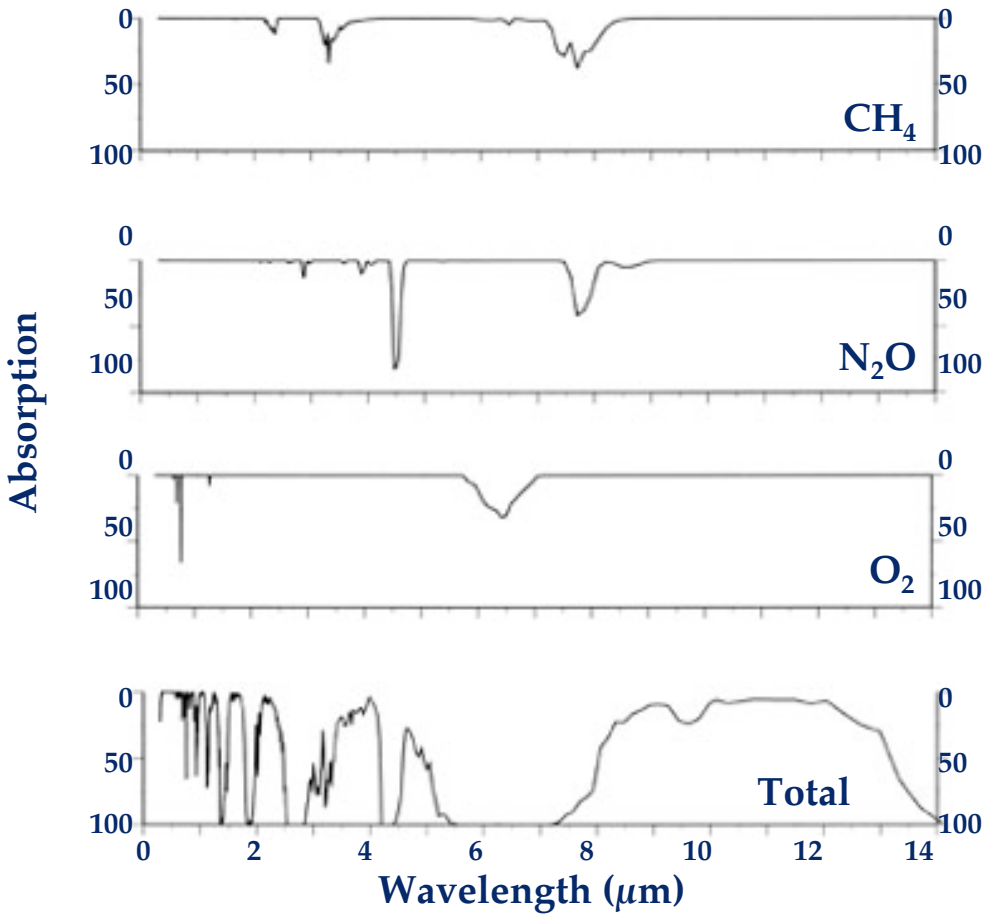

Figure 3.16b. Atmosphere absorption by atmosphere gases (con).

A consequence of these gaseous absorption processes is that we cannot remotely sense the Earth's surface in certain portions of the spectrum. Our observing capabilities become limited to certain spectral regions known as "atmospheric windows". Atmospheric windows are regions of the spectrum in which atmospheric transmission is sufficiently high that a significant amount of solar radiation is able to reach the terrestrial surface and be reflected towards the sensor (fig. 3.17). The main atmospheric windows are the following:

(i) the visible spectrum and near infrared, located between 0.3 and 1.35 □m;

(ii) several regions in the shortwave infrared from 1.5 to 1.8 □m, 2.0 to 2.4 □m, 2.9 to 4.2 □m, and 4.5 to 5.5 □m;

(iii) the thermal infrared, between 8 and 14 □m, and

(iv) the microwave region beyond 20 mm, where the atmosphere is practically transparent.

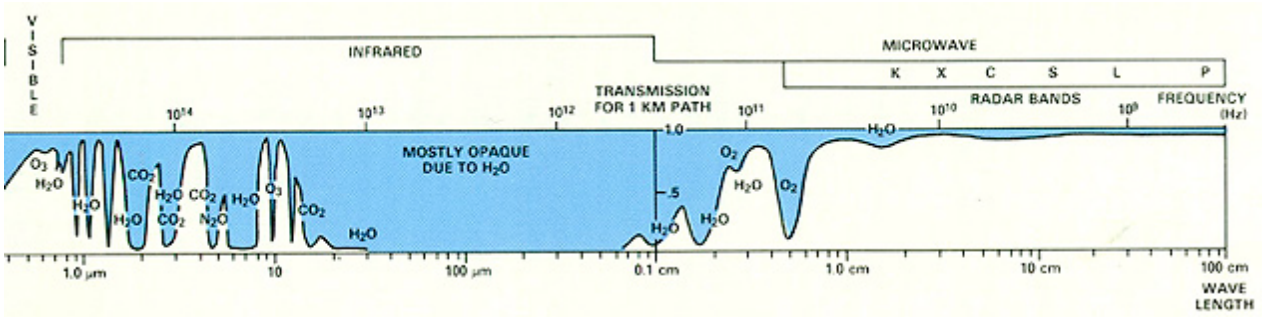

Figure 3.17. Atmosphere transmittance spectra and atmosphere "windows".

Thus, terrestrial based sensor systems are designed with spectral bandpasses that lie within these atmospheric windows in order to minimize sources of atmosphere contamination. Clouds are the exception in that they absorb throughout the optical spectrum and thus cannot be avoided. If we were interested in observing the atmosphere rather than the Earth's surface, then one would design the spectral bandpasses to lie within the spectral regions of maximum gaseous absorption. Meteorological satellites typically incorporate bands in such regions of the spectrum, e.g., band 2 of the Meteosat satellite was positioned between 5.7 and 7.1 □m, in order to study the water vapor content in the atmosphere (fig. 3.17), The Global Ozone Monitoring Experiment (GOME) sensor onboard the European satellite, ERS-2, and the Total Ozone Mapping Spectrometer (TOMS) have several bands in the ultraviolet for the purpose of monitoring the ozone layer.

Atmospheric scattering

In general, atmospheric gas absorption effects are best minimized through placement of spectral bandpasses where atmospheric transmittance is high. Atmospheric scattering, on the other hand, is more complex in that it occurs in all optical imagery acquired with remote sensing, regardless of bandpasses. The scattering of electromagnetic radiation is caused by its interaction with gaseous molecules and

atmospheric particles in suspension, namely aerosols and water vapor. An aerosol is a dispersion of solid particles (smoke, smog, and dust) and/or liquid particles (haze and fog) suspended in air and includes continental dust, oceanic salt spray, industrial activities, and biomass burning (figure 3.18). Aerosol size distributions vary markedly with cloud droplets generally >6 µm in size; dust particles, 1-3 µm and; smoke and anthropogenic aerosol particles are submicron (0.2 - 0.4 µm).

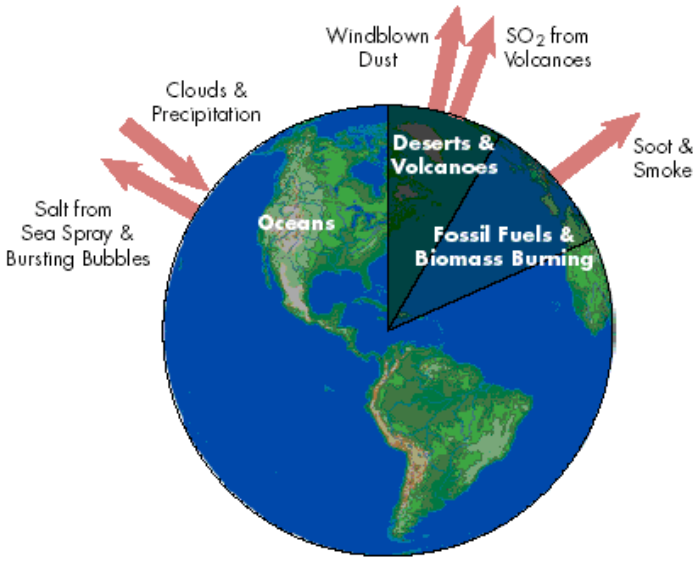

Figure 3.18. Sources of aerosols in the Earth's atmosphere.

Atmospheric particles scatter solar radiation in all directions creating an additional, diffuse irradiance component reaching the Earth's surface as well as an upward radiance component towards the sensor. As a result of scattering, the irradiance arriving at the surface has a direct (solar beam) and diffuse (sky) component. The diffuse component illuminates shadows and sunlit surfaces. On clear, dry days most of the irradiance is direct from the sun, with diffuse (sky) radiation making up as much as 10 - 15% of the sunlight. The more hazy (or turbid) the atmosphere, the stronger the diffuse, or sky, component and lower the direct, solar beam irradiance at the Earth's surface. Scattering within the atmosphere also creates an upward 'path radiance' that augments the signal received at the sensor.

Scattering is a function of the size of scattering particles relative to the wavelength and is generally stronger at shorter wavelengths. The scattering parameter, q, being related to the radius of the particles in the atmosphere, r, and wavelength of the solar radiation, λ according to:

$$q = 2\pi r / \lambda \qquad [3.2]$$

The manner in which the variable constituents in the atmosphere scatter solar radiation creates blue skies, red sunsets, and white and humid skies. There are three main types of scattering in the atmosphere:

- Rayleigh scattering involves molecules and other small particles with diameters much less than the incoming wavelengths of the radiation ($q<1$). Rayleigh scattering is responsible for the dominance of blue in a clear sky and for the atmosphere having a diffuse radiance. Variations in Rayleigh scattering are caused mostly by density fluctuations in the atmosphere (molecules).
- Mie scattering involves particles whose diameter approximate the wavelengths of incoming solar radiation (small water droplets and dust) ($1 < q < 2$). Aerosols and atmospheric dust are the main causes of this type of scattering, although it is also present in forest fires or coastal mists. This is found with slightly overcast skies and tends to influence longer wavelengths.
- Non-selective scattering involves particles with diameters several times the wavelength of incoming radiation (large water droplets, clouds and fog). This causes wavelengths of visible and near-infrared radiation to scatter with equal efficiency. As non-selective scattering affects various wavelengths in the same way, clouds and fog tend to appear white, since they scatter all the visible light in the same way.

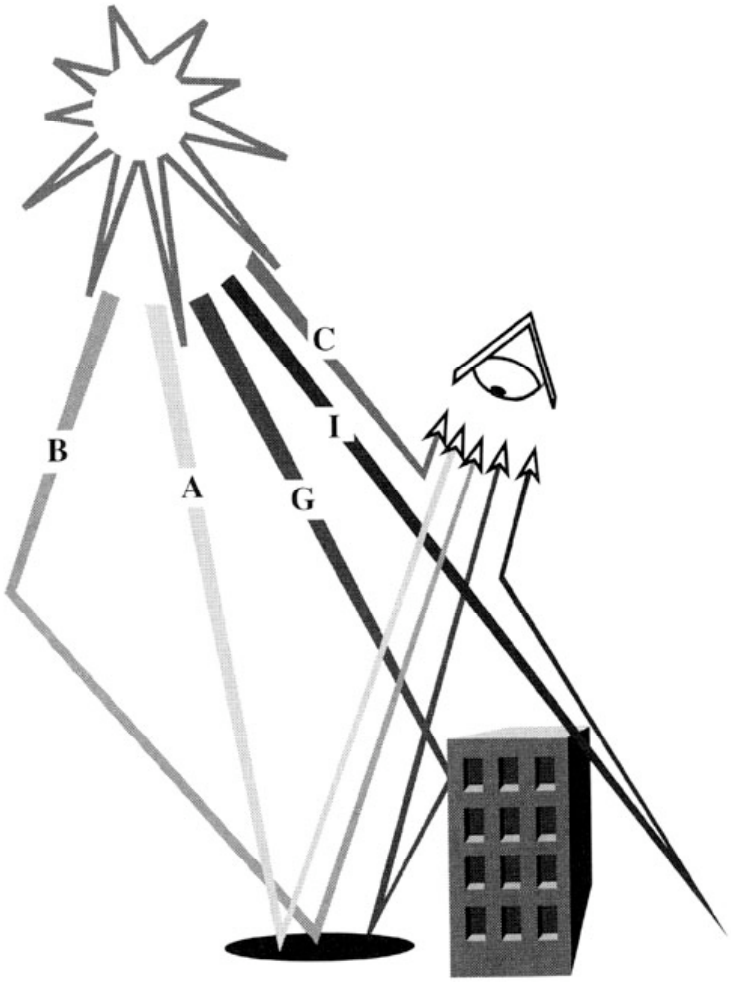

Figure 3.19. Influence of atmosphere scattering processes on the sensor signal. The scattering components may include (A) direct solar beam irradiance, (B) sky or diffuse irradiance, (C) upward path radiance, (G) background reflected objects, and (I) the adjacency effect.

Atmospheric scattering processes are very complex and difficult to quantify in remote sensing images. Aerosol amounts and composition are highly variable in time and space, making it difficult to quantify this influence in satellite remote sensing images. The atmosphere simultaneously reduces a surface reflected signal through a wavelength dependent transmission (attenuation) function, and adds its own atmospheric signal, known as the 'upward path' (sky) radiance (figure 3.19). Depending on the wavelength and the 'brightness' of the surface, as well as the turbidity of the atmosphere, the signal received at the sensor may be lower, higher, or unchanged relative to the ground signal. For a dark surface, atmospheric attenuation will be minimal but the path radiance contribution may far exceed the ground signal, particularly at shorter wavelengths. In

addition there is an adjacency effect whereby the surface leaving radiance from an adjacent pixel may be viewed within the pixel being observed (figure 3.19). Atmospheric corrections are particularly relevant in multitemporal remote sensing studies and when remotely-sensed data are being used to derive important surface biophysical parameters. The corrections for atmosphere scattering and absorption influences will be discussed later.

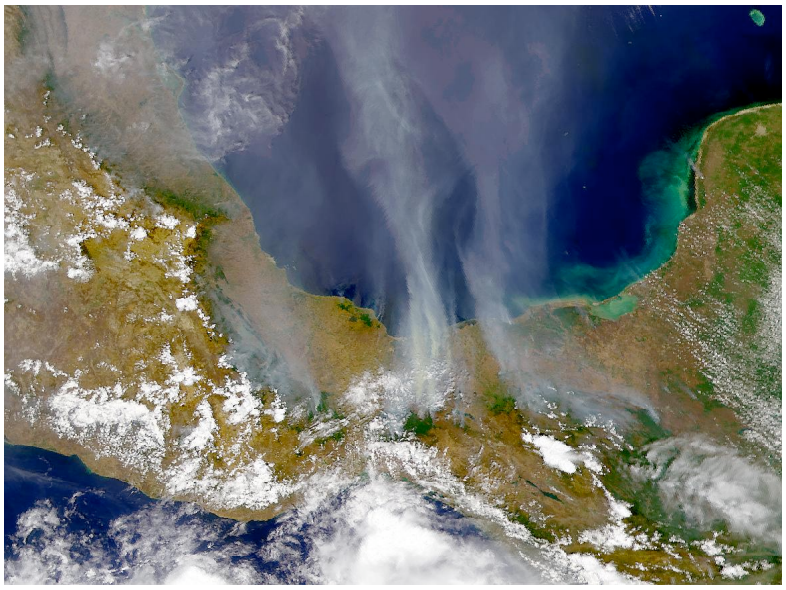

Figure 3.20. Fire plumes in Mexico as observed with the SeaWiFS sensor, June 5, 1998.

References

Aber, D.J., Wessman, C.A., Peterson, S.L., Melillo, J.M., and Fownes, J.H., 1990 Remote sensing of litter and soil organic matter decomposition in forest ecosystems, In: *Remote Sensing of Biosphere Functioning,* (R.J. Hobbs, H.A. Mooney, Eds.) Springer-Verlag, New York, pp. 87-101.

Asner, G.P. and Lobell, D.B., 2000, A biogeophysical approach for automated SWIR unmixing of soils and vegetation, *Remote Sensing of Environment,* 74:99-112.

Baumgardner, M.F., Silva, L.F., Biehl, L. L., and Stoner, E.R (1985). Reflectance properties of soils. *Advances in Agronomy,* 38:1-44.

Ben-Dor, E., Inbar, Y., and Chen, Y., 1997, The reflectance spectra of organic matter in the visible, near infrared and short wave infrared region (400-2500nm) during a control decomposition process, *Remote Sensing of Environment,* 61:1-15.

Ben-Dor, E., Irons, J.R., and Epema, G., 1999, Soil reflectance, p.111-188, IN A.N.Rencz (ed.) *Remote Sensing for the Earth Sciences*, John Wiley & Sons, Inc., New York.
Bhargava, D.S., and Mariam, D.W., 1990, Spectral reflectance relationships to turbidity generated by different clay materials, *Photogramm. Eng. and Remote Sensing*, 56:225-229.

Cohen, W.B., 1991, Response of vegetation indices to changes in in three measures of leaf water stress, *Photogramm, Eng. & Remote Sensing*, 57:195-202.

Colwell, J.E., 1974, Vegetation canopy reflectance, *Remote Sens. Environ*., 3:175-183.

Condit, H.R., 1970, The spectral reflectance of American soils, *PhotogrammetricEngineering,* 36:955-966.

Dozier, J., 1989, Spectral signature of alpine snow cover from Landsat Thematic Mapper, *Remote Sens. Environ*., 28:9-22.

Gates, D.M., Keegan, H.J., Schleter, J.C., and Weidner, V.R., 1965, Spectral properties of plants, *Applied Optics*, 4:11-20.

Hall, D.K., and Martinec, J., 1985, Remote Sensing of Ice and Snow, London, Chapman and Hall.

Hunt, E.R., and Rock, B.N., 1989, Detection of changes in leaf water content using near and middle-infrared reflectances, *Remote Sens. Environ*., 30:43-54.

Irons, J.R., Weismiller, R.A., and Petersen, G.W., 1989, Soil reflectance. P.66-106, In G.Asrar (ed*.) Theory and application of optical remote sensing*, John Wiley & Sons,New York.

Ji, W., Civco, D.L., and Kennard, W.C., 1992, Satellite remote bathymetry: a new mechanism for modeling, *Photogramm. Eng. & Remote Sensing*, 58:545-549.

Knipling, E.B., 1970, Physical and physiological basis for the reflectance of visible and near-infrared radiation from vegetation, *Remote Sens. Environ*., 1:155-159.

Liang, S., 1997, An investigation of remotely sensed soil depth in the optical region, Int.*Journal of Remote Sensing,* 18(16): 3395-3408.

Lopez, M.J., and Caselles, V., 1989, A multitemporal study of chlorophyll concentration in the Albufera Lagoon of Valencia, Spain using Thematic Mapper data, *Int. J. Remote Sensing*, 11:301-311.

McLellan, T.M., Aber, J.D., Martin, M.E., Melillo, J.M., and Nadelhoffer, K.J., 1991, Determination of nitrogen and cellulose content of decomposing leaf material by near infrared reflectance spectroscopy, *Canadian Journal Forrest Research,* 21:1684-1688.

Mulders, M.A., 1987, *Remote Sensing in Soil Science,* Amsterdam (Elsevier).

Musick, H.B., and Pelletier, R.E., 1988, Response to soil moisture of spectral indexes derived from bidirectional reflectance in Thematic Mapper wavebands, *Remote Sensing of Environment,* 25:167-184.

Nagler, P.L., Daughtry, C.S.T., Goward, S.N., 2000. Plant litter and soil reflectance, *Remote Sensing of Environment,* 71:207-215.

Stoner, E.R., and M.F. Baumgardner (1981). Characteristic variations in reflectance of surface soils. *Soil Science Society of American Journal,* 45: 1161-1165.

Tucker, C.J., 1979, Red and photographic infrared linear combinations for monitoringvegetation, *Remote Sensing of Environment,* 8:127-150.

Verhoef, W., 1984, Light scattering by leaf layers with application to canopy reflectance modeling: the SAIL model, *Remote Sens. Environ*., 16:125-141.

Westman, W.E., and Price, C.V., 1988, Spectral changes in conifers subjected to air pollution and water stress: experimental studies, *IEEE Trans. on Geoscience and Remote Sensing*, 26:11-20.

{Note – references are incomplete with respect to the atmosphere}
{Note 2 – the thermal and microwave sections are not yet complete)